PCCP

Accepted Manuscript

ROYAL SOCIETY OF CHEMISTRY

www.rsc.org/pccp

***Phys. Chem. Chem. Phys.*, 2014, Revised**

Hydrogen reversibility of $LiBH_4$-MgH_2-Al Composites

Bjarne R. S. Hansen[1], Dorthe B. Ravnsbæk[1,2], Jørgen Skibsted[3], Torben R. Jensen[1]*

[1] Center for Materials Crystallography, Interdisciplinary Nanoscience Center (iNANO), and Department of Chemistry, Aarhus University, Langelandsgade 140, DK-8000 Aarhus C, Denmark

[2] Massachusetts Institute of Technology, Department of Materials Science and Engineering, 77 Massachusetts Avenue, Cambridge, MA 02139, United States of America

[3] Instrument Centre for Solid-State NMR Spectroscopy, Department of Chemistry, and Interdisciplinary Nanoscience Center (iNANO), Aarhus University, Langelandsgade 140, DK-8000 Aarhus C, Denmark

* Corresponding author: Torben R. Jensen (trj@chem.au.dk)

***Phys. Chem. Chem. Phys.*, 2014, Revised**

ABSTRACT

The detailed mechanism for hydrogen release in $LiBH_4$−MgH_2−Al composites of molar ratios (4:1:1) and (4:1:5) are investigated during multiple cycles of hydrogen release and uptake. This study combines information from several methods, i.e., *in situ* synchrotron radiation powder X-ray diffraction, ^{11}B magic-angle spinning (MAS) NMR, Sieverts measurements, Fourier transform infrared spectroscopy and simultaneous thermogravimetric analysis, differential scanning calorimetry and mass spectroscopy. The composites of $LiBH_4$−MgH_2−Al are compared with the behavior of the $LiBH_4$−Al and $LiBH_4$−MgH_2 systems. The decomposition pathway of the $LiBH_4$−MgH_2−Al system is different for the two investigated molar ratios, although it ultimately results in formation of LiAl, $Mg_xAl_{1-x}B_2$ and $Li_2B_{12}H_{12}$ in both cases. For the 4:1:1-molar ratio, $Mg_{0.9}Al_{0.1}$ and $Mg_{17}Al_{12}$ are observed as intermediates. However, only Mg is observed as an intermediate in the 4:1:5-sample, which may be due to an earlier formation of $Mg_xAl_{1-x}B_2$, reflecting the complex chemistry of Al-Mg phases. Hydrogen release and uptake reveals a decrease in the hydrogen storage capacity upon cycling. This loss reflects the formation of $Li_2B_{12}H_{12}$ as observed by ^{11}B NMR and infrared spectroscopy for the cycled samples. Furthermore, it is shown that the $Li_2B_{12}H_{12}$ formation can be limited significantly by applying moderate hydrogen back pressure during decomposition.

Keywords: Hydrogen storage, reactive hydride composite systems, reversibility, $LiBH_4$-MgH_2-Al, $Li_2B_{12}H_{12}$.

***Phys. Chem. Chem. Phys.*, 2014, Revised**

1. INTRODUCTION

Hydrogen is suggested as a future carrier of renewable energy, however efficient, compact and safe storage is a challenging task.[1–3] For solid-state hydrogen storage, lightweight storage materials such as borohydrides, alanates and amidoboranes have received considerable attention, due to their large hydrogen densities, e.g., the gravimetric and volumetric hydrogen densities of $LiBH_4$ are 18.5 wt% H_2 and 120 kg H_2/m^3, respectively.[4–7] Unfortunately, poor thermodynamic and kinetic properties hamper the utilization of $LiBH_4$ in technological applications, primarily since it decomposes at temperatures above 375 °C due to the large enthalpy change, $\Delta H = -74$ kJ/mol H_2.[8–10] Furthermore, as a result of the formation of LiH during decomposition, only three quarters of the hydrogen content is available during decomposition (i.e., $\rho_m = 13.4$ wt% H_2) and temperatures above 600 °C as well as pressures above 155 bar H_2 are necessary for rehydrogenation of $LiBH_4$.[10] This may be due to formation of highly stable intermediate compounds such as lithium dodecahydro-*closo*-dodecaborate, $Li_2B_{12}H_{12}$ or amorphous boron.[11–17] Unfavorable decomposition properties and poor reversibility call for a better chemical insight and tailoring of the properties. One approach for improving the properties is to utilize reactive hydride composites (RHC), which leads to a more energetically favorable decomposition pathway.[18–31] This has been demonstrated for multiple composites, e.g., the $LiBH_4$–MgH_2 and $LiBH_4$–Al systems, for which the overall dehydrogenation and rehydrogenation reactions occur as shown in reactions 1-3.

$$2\ LiBH_4(s) + MgH_2(s) \rightarrow MgB_2(s) + 2\ LiH(s) + 4\ H_2(g) \quad (\mathbf{1})$$

$$2\ LiBH_4(s) + Al(s) \rightarrow AlB_2(s) + 2\ LiH(s) + 3\ H_2(g) \quad (\mathbf{2})$$

$$2\ LiH(s) + 2\ Al(s) \rightarrow 2\ LiAl(s) + H_2(g) \quad (\mathbf{3})$$

It has also been shown that a ternary composite of $LiBH_4$-MgH_2-Al lowers the decomposition temperature even further and that decomposition occurs by formation of $Mg_xAl_{1-x}B_2$ as shown in reaction 4: [32–34]

$$2LiBH_4(s) + xMgH_2(s) + (1\text{-}x)Al(s) \rightarrow 2LiH(s) + Mg_xAl_{1-x}B_2(s) + (4+x)H_2(g) \quad (\mathbf{4})$$

In the reactive hydride composites of $LiBH_4$-Al and $LiBH_4$-MgH_2, the decomposition takes place via a complex reaction mechanism involving several intermediates. However, for $LiBH_4$-MgH_2-Al the detailed mechanism is not yet fully understood. Therefore, the present investigation focuses on elucidating the detailed mechanism for multiple hydrogen release and uptake cycles in the ternary composite $LiBH_4$-MgH_2-Al system by *in situ* synchrotron radiation powder X-ray diffraction (SR-PXD), Sieverts method (PCT), thermo gravimetric analysis and differential scanning microscopy (TGA/DSC) coupled with mass spectroscopy (MS), solid-state ^{11}B magic-angle spinning (MAS NMR) and attenuated total reflectance Fourier transformed infrared spectroscopy (ATR-FTIR).

2. EXPERIMENTAL

2.1 Sample preparation. The chemicals lithium borohydride, $LiBH_4$ (Aldrich, ≥95%), aluminum, Al (Strem Chemicals, 99.7%) and MgH_2 (Aldrich) were purchased commercially and used without further purification. $LiBH_4$, MgH_2 and Al were mixed in the molar ratios 4:1:1 and 4:1:5, see Table 1. All handling was conducted under Argon atmosphere in a glove box equipped with circulation purifier (oxygen and water content both below 1 ppm). All samples were mechanically milled using a Fritsch Pulverisette No. 4, 80 mL tungsten carbide (WC) vials and 10 mm WC balls in a ball to powder mass ratio of approximately 35:1. All samples were milled for 5 min with 2 min intervals at a milling rate of 400 rpm (rounds per minute) under argon atmosphere, resulting in a total milling time of 120 min. Samples of $LiBH_4$-Al in molar ratios of 2:1 and 2:3, as well as a sample of $LiBH_4$-

MgH_2 in the molar ratio 2:1 were prepared under the same conditions and used for comparative measurements. Lithium *closo*-dodecahydro dodecaborane, $Li_2B_{12}H_{12}{\cdot}4H_2O$, purchased from Katchem, Prague, Czech Republic, was heated at T = 225 °C for 10 h under dynamic vacuum and used to obtain the anhydrous crystalline $Li_2B_{12}H_{12}$, according to previous work.[17]

2.2 Synchrotron Radiation Powder X-ray Diffraction (SR-PXD). *In situ* time resolved SR-PXD data was measured at beamline I711 at the synchrotron MAX-II, Lund, Sweden in the research laboratory MAX-Lab with a MAR165 CCD detector system.[35] The selected wavelengths were 1.10367 Å (sample **S1**) and 1.10113 Å (sample **S2**). The used sample cell was specially developed for studies of gas/solid reactions and allows variable pressures and temperatures to be applied.[36] The powdered samples were mounted in a sapphire single-crystal tube (Al_2O_3, outer diameter 1.09 mm, inner diameter 0.79 mm) inside an argon-filled glove box ($p(O_2, H_2O)$ < 1 ppm). The sample temperature was controlled with a thermocouple placed in the sapphire tube approximately 1 mm from the sample. A gas supply system was attached to the sample cell, which allowed a change in gas and pressure via a vacuum pump during the X-ray experiment. The system was flushed with argon and evacuated three times before the valve to the sample was opened and the X-ray experiment began. During desorption measurements the samples were heated to 535 °C with a heating rate of $\Delta T/\Delta t$ = 10 °C/min under dynamic vacuum (samples connected to a vacuum pump). The temperature was kept at 535 °C for 15 minutes before the samples were cooled to room temperature (*RT*). During absorption measurements the samples were heated to 400 °C ($\Delta T/\Delta t$ = 10 °C/min) under a pressure of $p(H_2)$ = 100 bar and kept at 400 °C for 1 hour before cooling to *RT* ($\Delta T/\Delta t$ = -10 °C/min). The FIT2D program was used to remove diffraction spots originating from the single-crystal sapphire tubes and subsequently to transform raw data to powder patterns.[37]

Rietveld refinement was performed on selected PXD data using the program Fullprof.[38] The backgrounds were described by linear interpolation between selected points, while pseudo-Voigt profile functions were used to fit the diffraction peaks. In general the unit cell parameters, zero shift, profile parameters and the overall temperature factors, B_{ov} were refined.

2.3 In house powder X-ray diffraction. In house PXD measurements were performed on a Rigaku Smartlab X-ray diffractometer equipped with a 180 mA and 40 kV Cu source (Cu Kα1 radiation, λ = 1.540593 Å, Cu Kα2 radiation, λ = 1.544414 Å) and a parallel beam multilayer mirror. Data was measured in the 2θ range 10 to 80° at 5°/min and obtained with a D/TeX Ultra detector. The sample was mounted in a 0.5 mm capillary (special glass # 0140 from Hilgenberg, Malsfeld, Germany) and sealed with glue in a mBraun Labmaster SP glovebox with Ar purifier ($p(O_2, H_2O) < 1$ ppm).

2.4 Sieverts measurement. A stainless steel autoclave was used for the Sieverts studies. The samples were transferred to the autoclave, which was sealed under argon atmosphere in a glove box ($p(O_2, H_2O) < 0.5$ ppm) and attached to the apparatus (Hy-Energy PCTPro-2000).[39] During desorption measurements the sample was heated to 300 °C ($\Delta T/\Delta t$ = 10 °C/min) and slowly heated from 300 to 500 °C ($\Delta T/\Delta t$ = 1 °C/min) at a backpressure of $p(H_2)$ = 0.15 bar and 5 bar, respectively. This temperature was maintained for 2.5 hours followed by natural cooling to *RT*. During hydrogen absorption measurements the sample was heated to 400 °C ($\Delta T/\Delta t$ = 5 °C/min) at $p(H_2)$ = 100 bar and cooled naturally to *RT* after 2.5 hours. After the first de- and absorption measurements the samples were characterized with PXD without exposure to air. Subsequently the samples were subjected to two additional hydrogen release and uptake cycles. Because of the high stoichiometric content of $LiBH_4$ in $LiBH_4$-MgH_2-Al (4:1:1, **S1**), the sample foams and some

material is lost. The amount of sample was determined gravimetrically after each desorption and absorption. Furthermore, it was necessary to grind the sample owing to sample hardening. After both desorption 1 and 2 and absorption 1 and 2, the $LiBH_4$-MgH_2-Al (4:1:1, **S1**) sample was ground by hand, since the powder was solidified during cooling, and further measurements could not be conducted without grinding. Thermal climbing and hardening is also observed for pristine $LiBH_4$, but it is only included for comparison, and not cycled. When a backpressure of $p(H_2)$ = 5 bar was applied during desorption, no additional grinding was needed.

2.5 Thermal analysis and Mass spectroscopy (TGA/DSC-MS). Thermo gravimetric analysis and differential scanning calorimetry (TGA/DSC) was measured using a PerkinElmer STA 6000 coupled with a mass spectrometer (MS) (Hiden Analytical HPR-20 QMS sampling system). The samples were transferred to Al_2O_3 crucibles under argon atmosphere in a glove box with circulation purifier (oxygen and water content both below 1 ppm). The samples were heated from 40 to 575 °C ($\Delta T/\Delta t$ = 5°C/min) with an argon purge rate of 65 mL/min. The outlet gaseous species, H_2 and B_2H_6, were monitored using mass spectroscopy.

2.6 ^{11}B-MAS NMR. ^{11}B MAS NMR spectra were obtained for $LiBH_4$-MgH_2-Al (4:1:1, **S1**) and $LiBH_4$-MgH_2-Al (4:1:5, **S2**) after ball milling and after three cycles of hydrogen release and uptake on a Varian Direct-Drive VNMRS-600 spectrometer (14.1 T) using a home-built CP/MAS NMR probe for a 4 mm outer diameter rotors. The experiments employed a spinning speed of ν_R = 12.0 kHz, a 0.5 μs excitation pulse for a ^{11}B rf field strength of $\gamma B_1/2\pi \approx 60$ kHz, a 4-s relaxation delay, and ^{1}H decoupling ($\gamma B_2/2\pi \approx 50$ kHz) during acquisition. The experiments were performed at ambient temperature using airtight end-capped zirconia rotors, which were packed with the samples

in an argon-filled glovebox. Isotropic chemical shifts are relative to neat $F_3B{\cdot}O(CH_2CH_3)_2$, employing a 0.1 M H_3BO_3 aqueous solution (δ_{iso} = 19.6 ppm) as a secondary, external standard sample.

2.7 Infrared spectroscopy. Infrared spectra were collected by Attenuated Total Reflectance - Fourier Transformed Infrared spectroscopy (ATR-FTIR), using a Nicolet 380 Avatar spectrometer. The sample powder was placed directly on the infrared radiation source and immediately covered by a tight screw. Thus, the total air exposure of the materials is limited to a few seconds. The spectra were collected in the wavenumber range of 4000 – 400 cm^{-1} with 32 scans.

3. RESULTS AND DISCUSSION

3.1 Thermal Decomposition.

The decomposition mechanism for the $LiBH_4$-MgH_2-Al composites **S1** and **S2** is investigated using *in situ* SR-PXD and thermal analysis. The *in situ* SR-PXD data for the desorption measurement of the $LiBH_4$-MgH_2-Al (4:1:1, **S1**) sample is presented in Figure 1a. The phase transformation of the orthorhombic $LiBH_4$ (*o*-$LiBH_4$) to the hexagonal polymorph of (*h*-$LiBH_4$) is observed at $T \approx 110$ °C. *h*-$LiBH_4$ melts at $T = 275$ °C. At $T \approx 310$ °C, the diffracted intensity from MgH_2 and Al decreases rapidly and diffraction peaks from $Mg_{17}Al_{12}$ appears. In addition, weak diffraction from $Mg_xAl_{1-x}B_2$ and possibly MgO is observed. This is shown in Figure 1b where integrated intensities of the phases observed in Figure 1a are presented. It should be noted that Bragg peaks from several phases (Al, $Mg_{17}Al_{12}$ and $Li_{0.3}Mg_{0.7}$) overlap in the temperature region 340-450 °C. The intensity

for these overlapping peaks at ~27° 2θ is denoted **X** in Figure 1b. The appearance of $Mg_{17}Al_{12}$ agrees well with previous reports[7,32–34] and with the Mg-Al phase diagram[40], i.e., as MgH_2 decomposes, the Al:Mg ratio changes from ~1:0 to ~1:1 and $Mg_{17}Al_{12}$ is expected to form in the region 52 – 59 mol% Al. At $T \approx 450$ °C, the diffraction peaks from $Mg_{17}Al_{12}$ vanishes and diffracted intensity from $Mg_{0.9}Al_{0.1}$ appears, which corresponds well with the melting point of $Mg_{17}Al_{12}$ (460 °C) as reported in the phase diagram.[40] Diffraction from $Mg_xAl_{1-x}B_2$ also increases in intensity in the temperature range 430 – 490 °C, simultanously with the formation of $Mg_{0.9}Al_{0.1}$ and remains constant during the remainder of the experiment. At $T = 500$ °C, diffraction from $Mg_{0.9}Al_{0.1}$ disappears completely and LiAl is formed (see eq. 3). Rietveld refinement of the diffractogram at $T \approx 360$ °C confirms that $Li_{0.3}Mg_{0.7}$, Al, $Mg_xAl_{1-x}B_2$ and $Mg_{17}Al_{12}$ are present, however, a clear composition determination is challenging owing to overlapping Bragg peaks. Rietveld refinement of a diffractogram measured at *RT* after desorption shows a sample composition of $Mg_xAl_{1-x}B_2$ (31.4 mol%), MgO (4.3 mol%), LiAl (16.1 mol%) and LiH (48.2 mol%). This agrees well with the expected composition for the idealized reaction (eq. 4). However, formation of MgO prohibits formation of $Mg_xAl_{1-x}B_2$, which may explain the appearance of LiAl, since the "free" Al that is not used in the formation of $Mg_xAl_{1-x}B_2$ can react with LiH, as observed in studies of the $LiBH_4$-Al and $LiBH_4$-$NaAlH_4$ systems.[16,28,29] This reaction occurs at low partial pressure of hydrogen and gives access to the full hydrogen content of the sample.

The *in situ* SR-PXD desorption measurement of $LiBH_4$-MgH_2-Al (4:1:5, **S2**) is presented in Figure 2a. The polymorphic transformation of *o*- to *h*-$LiBH_4$ is observed at $T = 110$ °C and *h*-$LiBH_4$ melts at $T = 275$ °C. Simultaneously with the melting of *h*-$LiBH_4$, a decrease in the intensity of peaks with contribution from Al is observed, which indicates that $LiBH_4$ reacts with Al. At $T \approx 295$ °C diffraction from MgH_2 disappears, after which diffracted intensity from Mg is observed. Bragg peaks from Mg, Al and LiH overlap, which is seen from the increase in the diffracted intensity of

the Al(+LiH) peak at 2θ = 27° in Figure 2b. The formation of $Mg_xAl_{1-x}B_2$ is observed at $T \approx 340$ °C which is at significantly lower temperature compared to $LiBH_4$-MgH_2-Al (4:1:1, **S1**) ($\Delta T \sim -90$ °C). This may be due to higher amounts of Al in sample **S2**, which may further destabilize $LiBH_4$. Another possible explanation for the earlier formation of $Mg_xAl_{1-x}B_2$ could be that the intermediate $Mg_{17}Al_{12}$ is not observed as expected according to the phase diagram for Al-Mg. LiAl is formed at $T = 450$ °C, again at a lower temperature compared to **S1** ($\Delta T \sim -50$ °C). At $T = 535$ °C, an unknown compound, denoted **3**, is observed. The diffracted intensity from **3** is constant throughout the remainder of the experiment, including the absorption measurement.

Data from the thermal analysis and MS during hydrogen desorption for samples **S1** and **S2** are presented in Figure 3 along with data for samples of $LiBH_4$-Al (2:3), $LiBH_4$-Al (2:1) and $LiBH_4$-MgH_2 (2:1) for comparison. The phase transformation and melting of $LiBH_4$ are observed in the DSC signal at approximately 110 and 275 °C for all samples, which agrees well with the *in situ* SR-PXD observations and with previously reported data.[41] The decomposition of MgH_2 for sample $LiBH_4$-MgH_2-Al (4:1:1, **S1**, red lines) is observed as an endothermic peak at $T = 300$ °C. This endotherm is not observed in the $LiBH_4$-MgH_2-Al (4:1:5, **S2**, black line) sample, although hydrogen release at $T = 300$ °C is detected in the MS data for both samples. A broad endothermic peak is observed in the DSC signal for **S2** in the temperature range 325 – 420 °C, simultaneously with a gradual gravimetric decrease in the TGA data and a continuous release of hydrogen observed by MS. The *in situ* SR-PXD measurements reveal that Mg and $Mg_xAl_{1-x}B_2$ form at $T \approx 315$ °C, hence the release of hydrogen could originate from the formation of these compounds. Another broad endotherm is observed for $LiBH_4$-MgH_2-Al (4:1:5, **S2**, black line) from 425 – 500 °C, which may reflect the formation of LiAl, as hydrogen is released in this temperature range as well. The total gravimetric mass loss for **S2** of 7.4 wt% is higher than the theoretically available hydrogen content of 7.3 wt%, possibly reflecting fluctuations during measurement. The $LiBH_4$-MgH_2-Al (4:1:1, **S1**,

red line) sample has an endothermic DSC event at T_{onset} = 375 °C, which originates from the formation of $Mg_xAl_{1-x}B_2$. This is also observed in the MS and TG data as a release of hydrogen and a gravimetric mass loss. The formation of LiAl is observed at T = 440 °C, however, less hydrogen is detected by MS as compared to $LiBH_4$-MgH_2-Al (4:1:5, **S2**, black line), which may indicate that less LiAl forms. The total gravimetric mass loss of $LiBH_4$-MgH_2-Al (4:1:1, **S1**) is 7.52 wt%, which corresponds to 75 % of the theoretically available hydrogen. No diborane was detected in either of the samples. It is noted that the hydrogen release in $LiBH_4$-MgH_2-Al (4:1:5, **S2**) is continuous, whereas the hydrogen release in $LiBH_4$-MgH_2-Al (4:1:1, **S1**) occurs in sharp separate steps confirming the markedly different desorption mechanism for the two samples observed by *in situ* SR-PXD. This also reflects that the formation of Mg-Al species in **S1** potentially hinders the reaction between Mg, Al and B, and therefore in **S2** the reaction between Mg, Al and B occurs at lower temperature since these Mg-Al species are not formed.

For comparison thermal analysis of $LiBH_4$-Al (2:1, **S3**), $LiBH_4$-Al (2:3, **S4**) and $LiBH_4$-MgH_2 (2:1, **S5**) was performed. This shows that the onset temperatures for hydrogen release in the $LiBH_4$-MgH_2-Al (4:1:1, **S1**) and $LiBH_4$-MgH_2-Al (4:1:5, **S2**) samples are lowered by approximately 100, 50 and 75 °C as compared to **S3**, **S4** and **S5**, respectively, in agreement with previous work.[32] The onset and peak temperatures for the hydrogen release, T_{onset} and T_{peak}, seem to be related to the amounts of Al in the composite (see Table 2), i.e., the larger the stoichiometric amounts of Al, the lower is the hydrogen desorption temperature.

3.2 Hydrogen absorption.

The *in situ* SR-PXD data measured during hydrogen absorption of $LiBH_4$-MgH_2-Al (4:1:1, **S1**) is presented in Figure 4. During heating to 400 °C (Figure 4a) diffracted intensity from LiAl disappears at $T \approx 250$ °C and diffraction from Al is observed, i.e., the reverse of reaction eq. 3.

Similarly diffracted intensity from $Mg_xAl_{1-x}B_2$ disappears at $T \approx 370$ °C, simultaneously with formation of Mg and a further increase in diffracted intensity from Al. For a few scans an unknown phase is observed (denoted **1**). Magnesium is quickly hydrogenated to form MgH_2 that is visible throughout the remainder of the measurement. Hence, the magnesium aluminum alloy intermediates observed during desorption are not observed during absorption, likely owing to the fast formation of MgH_2, which prevents formation of any Al-Mg phases. During cooling (Figure 4b) *h*-$LiBH_4$ crystallizes from the melt at approximately 270 °C and the transformation to *o*-$LiBH_4$ is observed at $T \approx 100$ °C. Another unknown phase is observed (denoted **2**). During cooling a broad peak from MgO is also observed. It should be noted that the diffraction rings from $LiBH_4$ appear "spotty", i.e., poor powder average, which results in the small variations in diffracted intensities from MgH_2 and $LiBH_4$ from scan to scan. This is likely due to particle growth during crystallization. ESI data for the unknown compounds **1**, **2**, and **3** is provided in Table S2 (Supporting Information).

The absorption measurement for $LiBH_4$-MgH_2-Al (4:1:5, **S2**) is presented in Figure 5. At approximately $T \approx 350$ °C diffracted intensity from LiAl and $Mg_xAl_{1-x}B_2$ disappears, and diffracted intensity from Al is observed, corresponding to the reaction:

$$4LiAl(s) + 2Mg_xAl_{1-x}B_2(s) + (8+2x)H_2(g) \rightarrow 4LiBH_4(l) + 2xMgH_2(l) + (6-2x)Al(s) \qquad (\mathbf{5})$$

During cooling MgH_2 and *h*-$LiBH_4$ crystallizes from the melt at $T \approx 285$ °C and $T \approx 270$ °C, respectively. The phase transformation from *h*- to *o*-$LiBH_4$ is observed at $T \approx 100$ °C. No diffraction from MgO is observed, as detected for the $LiBH_4$-MgH_2-Al (4:1:1, **S1**) sample. The system is reversible at the applied physical conditions and Rietveld refinements of the data collected before desorption and after absorption (Table 3) show that approximately 55 % $LiBH_4$ and 98 % MgH_2 is reformed after ~1 hour of hydrogenation (Rietveld plots and crystallographic data is shown

in supporting information). It should be noted that $LiBH_4$ reformation could possibly be increased using longer rehydrogenation times.

3.3 Reversibility of hydrogen release and uptake.

The reversibility of **S1** and **S2** is investigated using Sieverts measurements, ^{11}B MAS NMR and IR spectroscopy. Sieverts hydrogen desorption measurements of $LiBH_4$-MgH_2-Al (4:1:1, **S1**, red curve), $LiBH_4$-MgH_2-Al (4:1:5, **S2**, black curve) and pristine $LiBH_4$ are presented in Figure 6. The first desorption of **S1** shows gas release in two separate steps, with a total release of 9.7 wt%, which agrees very well with the theoretically available hydrogen content (ρ_m = 10.0 wt% H_2). The first hydrogen release step is possibly related to the decomposition of MgH_2 at $T \approx 280$ °C. The second step releases hydrogen in the temperature range T = 295 – 400 °C, which reflects the formation of $Mg_xAl_{1-x}B_2$ that is formed by a reaction between $LiBH_4$, Al and Mg. Hydrogen release related to the formation of LiAl is not observed. This reaction step is not expected from the molar composition of the sample, however, LiAl was detected during the *in situ* SR-PXD measurements. A possible reason for this is the dynamic vacuum applied during the *in situ* SR-PXD, which may promote the reaction between LiH and Al,[30] as opposed to the static vacuum employed for the Sievert's measurements. Similar effects have been observed previously in a study of $LiBH_4$-Al.[16] In Figure 7 diffractograms after desorption and absorption of **S1** are presented. After desorption $Mg_xAl_{1-x}B_2$ and Al are detected, which are the expected decomposition products. After the first absorption $LiBH_4$, MgH_2 and Al are observed, however, the diffracted intensity of $LiBH_4$ is weaker compared to the ball milled sample (BM), which suggests that less $LiBH_4$ is present after three hydrogen cycles. This observation is also confirmed by the Sieverts data in Figure 6, since less hydrogen is released in the second and third desorption compared to the first. Hence, the hydrogen storage capacity decreases. Desorption 3 releases 6.2 wt%, i.e., 64 % of that observed during desorption 1. The difference in pressure at *RT* before and after the Sieverts hydrogen absorption experiments allows

calculation of the hydrogen uptake (see Table 4). Indeed it shows that the hydrogen uptake is limited, but most of the absorbed hydrogen is released in the subsequent desorption (absorption 2 takes up 6.4 wt% H_2 and desorption 3 release 6.2 wt% H_2).

The first desorption measurement for $LiBH_4$-MgH_2-Al (4:1:5, **S2**, black lines) shows a total hydrogen release of 6.4 wt% corresponding to 88.9 % of the total hydrogen content. At $T \approx 265$ °C a small hydrogen gas release is observed as a result of the decomposition of MgH_2. In the temperature range $T = 300 – 380$ °C, a large gas release is observed from the formation of $Mg_xAl_{1-x}B_2$, similar to that observed for $LiBH_4$-MgH_2-Al (4:1:1, **S1**). At $T = 440$ °C, another gas release is observed, which originates from the formation of LiAl, in accord with *in situ* SR-PXD and thermal analysis. Diffractograms of $LiBH_4$-MgH_2-Al (4:1:5, **S2**) measured after desorption in the Sieverts apparatus (Figure 7) confirm the hydrogen release steps observed in Figure 6, since LiAl, $Mg_xAl_{1-x}B_2$ and Al are detected, which are the expected decomposition products. LiAl is likely hydrogenated by the moderate hydrogen pressure in the setup after desorption, which may explain the formation of Al. Similar observations are documented in a previous study.[16] After the first absorption, $LiBH_4$, MgH_2 and Al are observed together with diffraction from **3**. As in **S1** the diffracted intensity of $LiBH_4$ is weaker compared to the ball milled sample (BM) and PCT desorptions 2 and 3 also show a decrease in hydrogen storage capacity (see Table 4). The release step related to the formation of $Mg_xAl_{1-x}B_2$ is decreasing significantly, compared to the steps related to MgH_2 decomposition and formation of LiAl that are nearly constant for all three desorptions. This is also observed in the **S1** desorptions. Hence, the capacity loss is possibly related to formation of $Mg_xAl_{1-x}B_2$ or $LiBH_4$, i.e., a boron-containing compound. As expected, **S2** shows the same decrease in the absorbed amounts of H_2.

PCT desorption of pristine $LiBH_4$ is performed to compare with **S1** and **S2** and shown in blue in Figure 6. It is clear that the temperature for the main hydrogen release is lowered by $\Delta T \approx 100$ °C in **S1** and **S2** compared to $LiBH_4$. The gas release from $LiBH_4$ is ~10.5 wt%, which indicates that only partial decomposition is achieved at 500 °C. In Figure 7(d) and (e) diffractograms of **S1** and **S2** after three hydrogen release and uptake cycled are presented. These diffractograms show weak Bragg peaks from $LiBH_4$, which underlines the loss of hydrogen storage capacity observed in the PCT desorption. Diffraction from MgH_2 in **S1** shows increasing intensity as compared to the ball-milled sample, which may reflect particle growth, in accord with the *in situ* SR-PXD absorption measurements.

3.4 Hydrogen release under different conditions

In order to investigate effects of hydrogen partial pressure, samples **S1** and **S2** were subjected to three hydrogen release and uptake cycles in a Sieverts apparatus using $p(H_2) = 5$ bar during decomposition. These data is compared to those obtained with a partial pressure of $p(H_2) = 0.15$ bar presented above. All other conditions were similar for these Sieverts measurements. ^{11}B MAS NMR spectra were acquired for the ball milled samples and the samples of **S1** and **S2** after three hydrogen de- and absorption PCT cycles with different hydrogen partial pressure (Figures 8 and 9). For the ball milled samples only the centerband resonance at –41.3 ppm from $LiBH_4$ and its associated spinning sidebands are observed for the **S1** and **S2** samples (spectra not shown). Centerband resonances from both $LiBH_4$ and $Li_2B_{12}H_{12}$ are observed for the cycled samples of **S1** (Figure 8) and **S2** (Figure 9), where $Li_2B_{12}H_{12}$ exhibits a broadened resonance at –9 ppm, as observed for a pure sample of this phase (Figure 8c). $Li_2B_{12}H_{12}$ is a stable *closo*-borane and its formation may be a reason for the loss of hydrogen storage capacity upon cycling. The relative fractions of $LiBH_4$ and $Li_2B_{12}H_{12}$ have been determined from the intensities of the resonances from the ^{11}B central and satellite transitions for $LiBH_4$ and the central transition intensity only for $Li_2B_{12}H_{12}$, and are

summarized in Table 5. These data shows that a larger amount of $Li_2B_{12}H_{12}$ is formed in the $LiBH_4$-MgH_2-Al (4:1:1, **S1**) sample as compared to $LiBH_4$-MgH_2-Al (4:1:5, **S2**), possibly reflecting the presence of more $LiBH_4$ in **S1**. Furthermore, it is clear that less $Li_2B_{12}H_{12}$ is formed in the samples cycled with $p(H_2)$ = 5 bar, which increases the reversible hydrogen storage capacity of the RHC-system. Remarkably, 97.6 mol% $LiBH_4$ is left after three hydrogen cycles in **S2** using $p(H_2)$ = 5 bar during desorption, however, some boron loss may have occurred during the hydrogen cycles.

Formation of $Li_2B_{12}H_{12}$ is also confirmed by FT-IR and spectra of samples **S1** and **S2** after ball milling and three hydrogen release and uptake cycles ($p(H_2)$ = 0.15 bar) are presented in Figure 10. All samples show resonant frequencies in the 2400-2195 cm^{-1} region and at 1054 cm^{-1}, which are assigned to B-H stretching and bending modes for $LiBH_4$, respectively.[42,43] In the cycled samples a peak at 2450 cm^{-1} is observed, which is assigned to vibrational modes in the $B_{12}H_{12}^{2-}$ anion that originate from $Li_2B_{12}H_{12}$.[44–47] $Li_2B_{12}H_{12}$ is also observed in the samples of **S1** and **S2** after three hydrogen release and uptake cycles using $p(H_2)$ = 5 bar (spectra not shown). MgH_2 is observed in all samples by the broad peak in the 500-700 cm^{-1} region. The ball-milled samples show also a broad peak, which may be assigned to O-H stretching modes, indicating that the samples have been exposed to air prior to the FT-IR measurements.

$Li_2B_{12}H_{12}$ is not observed by PXD, however, data obtained from the samples cycled with 5 bar H_2 indicate that a larger amount of $LiBH_4$ is reversibly formed in both samples as compared to those decomposed at lower partial pressure, $p(H_2)$ = 0.15 bar, (see Figure 11). The fact that more $LiBH_4$ is formed at high $p(H_2)$ may reflect a decrease in the formation of $Li_2B_{12}H_{12}$, which is verified by ^{11}B MAS NMR. It is also observed from X-ray diffraction that the samples decompose fully, even at $p(H_2)$ = 5 bar, since the expected decomposition products are observed. Unknown compound **3** is detected in all four cases, but it is more pronounced in the samples cycled at $p(H_2)$ = 0.15 bar.

Pristine $LiBH_4$ decomposes to increasing amounts of amorphous boron and decreasing amounts of $Li_2B_{12}H_{12}$ for decreasing partial pressures of hydrogen.[48] Lithium borohydride RHC's containing metals such as calcium, yttrium or cerium reveal decomposition to increasing amounts of metal borides for increasing $p(H_2)$.[49,50] Similar behavior is observed for the $LiBH_4$-MgH_2-Al composites investigated in this study, since smaller amounts of $Li_2B_{12}H_{12}$ are observed at higher $p(H_2)$. Thus, these investigations suggest that formation of *closo*-borane is limited under these conditions.

It is noteworthy that $Li_2B_{12}H_{12}$ is formed but no B_2H_6 has been detected by MS during the TGA-DSC-MS measurements in any samples. Previous reports reveal that $LiBH_4$ may release B_2H_6 during decomposition and that $LiBH_4$ and B_2H_6 reacts during reactive ball milling and form $Li_2B_{12}H_{12}$.[14] In this investigation, B_2H_6 may also be released during decomposition of $LiBH_4$ but it reacts immediately with remaining $LiBH_4$ forming $Li_2B_{12}H_{12}$.

5. CONCLUSION

$LiBH_4$-MgH_2-Al composites were prepared mechanochemically in molar ratios 4:1:1 and 4:1:5. The decomposition reactions in the two $LiBH_4$-MgH_2-Al samples were investigated using *in situ* SR-PXD and TG/DSC-MS. Furthermore, the reversibility was studied during multiple cycles of hydrogen release and uptake using Sieverts measurements at different hydrogen backpressures, ^{11}B MAS NMR, and IR spectroscopy. The decomposition of $LiBH_4$-MgH_2-Al (4:1:1, **S1**) is complex and occurs with several intermediates, i.e., $Mg_{0.9}Al_{0.1}$ and $Mg_{17}Al_{12}$, before $Mg_xAl_{1-x}B_2$ and LiAl is formed. In contrast, no Mg-Al intermediates were observed in the $LiBH_4$-MgH_2-Al (4:1:5, **S2**) sample, and $Mg_xAl_{1-x}B_2$ and LiAl was formed at much lower temperatures compared to $LiBH_4$-MgH_2-Al (4:1:1, **S1**) ($\Delta T \sim 90$ and 50 °C, respectively). Compared to the $LiBH_4$-Al and $LiBH_4$-MgH_2 systems, the decomposition temperature is lowered by approximately 75 °C in both $LiBH_4$-

MgH_2-Al (4:1:1) and (4:1:5) in accordance with previous work.[32] The hydrogen storage capacity decreases during repeated hydrogen release and uptake cycles, possibly due to the gas release step related to the formation of $Mg_xAl_{1-x}B_2$ and reformation of $LiBH_4$. Formation of $Li_2B_{12}H_{12}$ was determined by ^{11}B MAS NMR and FTIR, which is highly stable and contribute to the decrease in hydrogen storage capacity. We demonstrate that the formation of $Li_2B_{12}H_{12}$ can be limited by applying moderate hydrogen backpressures during hydrogen release, which in addition preserves the hydrogen storage capacity.

ACKNOWLEDGEMENTS

The work was supported by The Danish Council for Strategic Research (the research project HyFillFast), the Danish National Research Foundation, Center for Materials Crystallography (DNRF93), and by the Danish Research Council for Nature and Universe (Danscatt). We are grateful to the Carlsberg Foundation. We also acknowledge funding from the European Community's Seventh Framework Programme, The Fuel Cells and Hydrogen Joint Undertaking (FCH JU), project BOR4STORE (303428) and the COST Action MP1103 "Nanostructured materials for solid-state hydrogen storage". The access to beamtime at the MAX-II synchrotron, Lund, Sweden in the research laboratory MAX-lab is gratefully acknowledged. The use of the facilities at the Instrument Centre for Solid-State NMR Spectroscopy, Department of Chemistry, Aarhus University, sponsored by the Danish Natural Science Research Councils and the Carlsberg Foundation is acknowledged.

REFERENCES

1. L. Schlapbach and A. Züttel, *Nature*, 2001, **414**, 353–358.
2. L. Schlapbach, *Nature*, 2009, **460**, 809–811.
3. U. Eberle, M. Felderhoff, and F. Schüth, *Angew. Chem. Int. Ed.*, 2009, **48**, 6608–6630.
4. D. B. Ravnsbæk, Y. Filinchuk, R. Cerný, and T. R. Jensen, *Z. Krist.*, 2010, **225**, 557–569.
5. L. H. Rude, T. K. Nielsen, D. B. Ravnsbæk, U. Bösenberg, M. B. Ley, B. Richter, L. M. Arnbjerg, M. Dornheim, Y. Filinchuk, F. Besenbacher, and T. R. Jensen, *Phys. Status Solidi A*, 2011, **208**, 1754–1773.
6. F. E. Pinkerton, G. P. Meisner, M. S. Meyer, M. P. Balogh, and M. D. Kundrat, *J Phys Chem B*, 2005, **109**, 6–8.
7. J. Mao, Z. Guo, H. Leng, Z. Wu, Y. Guo, X. Yu, and H. Liu, *J. Phys. Chem. C*, 2010, **114**, 11643–11649.
8. J.-P. Soulié, G. Renaudin, R. Černý, and K. Yvon, *J. Alloys Comp.*, 2002, **346**, 200–205.
9. A. Züttel, S. Rentsch, P. Fischer, P. Wenger, P. Sudan, P. Mauron, and C. Emmenegger, *J. Alloys Comp.*, 2003, **356–357**, 515–520.
10. A. Remhof, O. Friedrichs, F. Buchter, P. Mauron, J. W. Kim, K. H. Oh, A. Buchsteiner, D. Wallacher, and A. Züttel, *J. Alloys Comp.*, 2009, **484**, 654–659.
11. S.-J. Hwang, R. C. Bowman, J. W. Reiter, Rijssenbeek, G. L. Soloveichik, J.-C. Zhao, H. Kabbour, and C. C. Ahn, *J. Phys. Chem. C*, 2008, **112**, 3164–3169.
12. S.-I. Orimo, Y. Nakamori, N. Ohba, K. Miwa, M. Aoki, S. Towata, and A. Züttel, *Appl. Phys. Lett.*, 2006, **89**, 021920–021920–3.
13. N. Ohba, K. Miwa, M. Aoki, T. Noritake, S. Towata, Y. Nakamori, S. Orimo, and A. Züttel, *Phys. Rev. B*, 2006, **74**, 075110.
14. O. Friedrichs, A. Remhof, S.-J. Hwang, and A. Zu□ttel, *Chem. Mater.*, 2010, **22**, 3265–3268.
15. V. Ozolins, E. H. Majzoub, and C. Wolverton, *J. Am. Chem. Soc.*, 2009, **131**, 230–237.
16. B. R. S. Hansen, D. B. Ravnsbæk, D. Reed, D. Book, C. Gundlach, J. Skibsted, and T. R. Jensen, *J. Phys. Chem. C*, 2013, **117**, 7423–7432.
17. M. P. Pitt, M. Paskevicius, D. H. Brown, D. A. Sheppard, and C. E. Buckley, *J. Am. Chem. Soc.*, 2013, **135**, 6930–6941.

18. U. Bösenberg, S. Doppiu, L. Mosegaard, G. Barkhordarian, N. Eigen, A. Borgschulte, T. R. Jensen, Y. Cerenius, O. Gutfleisch, T. Klassen, M. Dornheim, and R. Bormann, *Acta Mater.*, 2007, **55**, 3951–3958.

19. T. E. C. Price, D. M. Grant, V. Legrand, and G. S. Walker, *Int. J. Hydrogen Energy*, 2010, **35**, 4154–4161.

20. P. Sridechprasat, Y. Suttisawat, P. Rangsunvigit, B. Kitiyanan, and S. Kulprathipanja, *Int. J. Hydrogen Energy*, 2011, **36**, 1200–1205.

21. J. Yang, A. Sudik, and C. Wolverton, *J. Phys. Chem. C*, 2007, **111**, 19134–19140.

22. D. Blanchard, Q. Shi, C. B. Boothroyd, and T. Vegge, *J. Phys. Chem. C*, 2009, **113**, 14059–14066.

23. O. Friedrichs, J. W. Kim, A. Remhof, F. Buchter, A. Borgschulte, D. Wallacher, Y. W. Cho, M. Fichtner, K. H. Oh, and A. Züttel, *Phys. Chem. Chem. Phys.*, 2009, **11**, 1515.

24. S.-A. Jin, J.-H. Shim, Y. W. Cho, K.-W. Yi, O. Zabara, and M. Fichtner, *Scr. Mater.*, 2008, **58**, 963–965.

25. X.-D. Kang, P. Wang, L.-P. Ma, and H.-M. Cheng, *Appl. Phys. A*, 2007, **89**, 963–966.

26. J. W. Kim, O. Friedrichs, J.-P. Ahn, D. H. Kim, S. C. Kim, A. Remhof, H.-S. Chung, J. Lee, J.-H. Shim, Y. W. Cho, A. Züttel, and K. H. Oh, *Scr. Mater.*, 2009, **60**, 1089–1092.

27. H.-W. Li, Y. Yan, S. Orimo, A. Züttel, and C. M. Jensen, *Energies*, 2011, **4**, 185–214.

28. D. B. Ravnsbæk and T. R. Jensen, *J. Appl. Phys.*, 2012, **111**, 112621–112621–9.

29. D. B. Ravnsbæk and T. R. Jensen, *J. Phys. Chem. Solids*, 2010, **71**, 1144–1149.

30. T. E. C. Price, D. M. Grant, D. Weston, T. Hansen, L. M. Arnbjerg, D. B. Ravnsbæk, T. R. Jensen, and G. S. Walker, *J. Am. Chem. Soc.*, 2011, **133**, 13534–13538.

31. M. Meggouh, D. M. Grant, and G. S. Walker, *J. Phys. Chem. C*, 2011, **115**, 22054–22061.

32. Y. Zhang, Q. Tian, H. Chu, J. Zhang, L. Sun, J. Sun, and Z. Wen, *J. Phys. Chem. C*, 2009, **113**, 21964–21969.

33. T. K. Nielsen, U. Bo□senberg, R. Gosalawit, M. Dornheim, Y. Cerenius, F. Besenbacher, and T. R. Jensen, *ACS Nano*, 2010, **4**, 3903–3908.

34. Y. Li, T. Izuhara, and H. T. Takeshita, *Materials Transactions*, 2011, **52**, 641–646.

35. Y. Cerenius, K. Ståhl, L. A. Svensson, T. Ursby, Å□;. Oskarsson, J. Albertsson, and A. Liljas, *J. Synchrotron Radiat.*, 2000, **7**, 203–208.

36. T. R. Jensen, T. K. Nielsen, Y. Filinchuk, J.-E. Jørgensen, Y. Cerenius, E. M. Gray, and C. J. Webb, *J. Appl. Cryst.*, 2010, **43**, 1456–1463.

37. A. P. Hammersley, S. O. Svensson, M. Hanfland, A. N. Fitch, and D. Hausermann, *High Pres. Res.*, 1996, **14**, 235–248.

38. J. Rodríguez-Carvajal, *Phys. B*, 1993, **192**, 55–69.

39. Y.-W. Lee, B. M. Clemens, and K. J. Gross, *J. Alloys Comp.*, 2008, **452**, 410–413.

40. Y. Zhong, M. Yang, and Z.-K. Liu, *Calphad*, 2005, **29**, 303–311.

41. L. Mosegaard, B. Møller, J.-E. Jørgensen, U. Bösenberg, M. Dornheim, J. C. Hanson, Y. Cerenius, G. Walker, H. J. Jakobsen, F. Besenbacher, and T. R. Jensen, *J. Alloys Comp.*, 2007, **446–447**, 301–305.

42. G. Socrates, *Infrared and Raman Characteristic Group Frequencies: Tables and Charts*, Wiley, 2004.

43. V. D'Anna, A. Spyratou, M. Sharma, and H. Hagemann, *Spectrochim Acta A*, Manuscript Number: SAA–D–13–02143.

44. J. Mao, Z. Guo, H. Leng, Z. Wu, Y. Guo, X. Yu, and H. Liu, *J. Phys. Chem. C*, 2010, **114**, 11643–11649.

45. J. Mao, Z. Guo, I. P. Nevirkovets, H. K. Liu, and S. X. Dou, *J. Phys. Chem. C*, 2012, **116**, 1596–1604.

46. E. L. Muetterties, R. E. Merrifield, H. C. Miller, W. H. Knoth, and J. R. Downing, *J. Am. Chem. Soc.*, 1962, **84**, 2506–2508.

47. J. Mao, Z. Guo, H. Liu, and S. X. Dou, *J. Mater. Chem. A*, 2012.

48. Y. Yan, A. Remhof, S.-J. Hwang, H.-W. Li, P. Mauron, S. Orimo, and A. Züttel, *Phys. Chem. Chem. Phys.*, 2012, **14**, 6514–6519.

49. J.-H. Shim, J.-H. Lim, S. Rather, Y.-S. Lee, D. Reed, Y. Kim, D. Book, and Y. W. Cho, *J. Phys. Chem. Lett.*, 2010, **1**, 59–63.

50. K.-B. Kim, J.-H. Shim, Y. W. Cho, and K. H. Oh, *Chem. Commun.*, 2011, **47**, 9831–9833.

Table 1. Composition of the $LiBH_4$-MgH_2-Al, $LiBH_4$-Al and $LiBH_4$-MgH_2 samples and the gravimetric hydrogen contents for the investigated samples, $\rho_m(H_2)$.

		Composition (mol %)			$\rho_m(H_2)$
Name	**Content**	**$LiBH_4$**	**MgH_2**	**Al**	**wt%**
S1	$LiBH_4$-MgH_2-Al (4:1:1)	66.7	16.7	16.7	10.0
S2	$LiBH_4$-MgH_2-Al (4:1:5)	40.0	10.0	50.0	7.2
S3*	$LiBH_4$-Al (2:1)	66.7	-	33.3	11.3
S4*	$LiBH_4$-Al (2:3)	40.0	-	60.0	6.4
S5*	$LiBH_4$-MgH_2 (2:1)	66.7	33.3	-	14.3

* The samples are only used comparatively in thermal analysis.

Table 2. Thermal events and gravimetric mass loss observed by TGA-DSC-MS presented in Figure 3. *

Sample	T_{onset} (°C)	T_{peak} (°C)	T_{end} (°C)	$\Delta m/m$ (%)
$LiBH_4$-Al (2:1)	380	425	455	8.4
$LiBH_4$-Al (2:3)	325	375	450	6.1
$LiBH_4$-MgH_2 (2:1)	350	420	440	11.3
$LiBH_4$-MgH_2-Al (4:1:1)	275	415	440	7.5
$LiBH_4$-MgH_2-Al (4:1:5)	275	400	485	7.5

* The onset for hydrogen release (T_{onset}), the temperature for maximum hydrogen release (T_{peak}), and the end of the thermal event (T_{end}), are extracted from the MS data along with the mass loss obtained for the same temperature range from TGA data.

Table 3. Fractional composition of $LiBH_4$-MgH_2-Al (4:1:5, **S2**) before desorption and after absorption.*

	Before desorption		After Absorption		Theoretical
Compound	**wt%***	**mol%**	**wt%***	**mol%**	**mol%**
$LiBH_4$	39.44	44.58	20.76	24.46	40.00
MgH_2	7.13	6.67	6.72	6.55	10.00
Al	53.42	48.75	72.52	68.99	50.00

*The fractional compositions (wt%) are extracted by Rietveld refinement and used to calculate the molar ratio (mol%). Diffraction originating from **3** is neglected.

Table 4. Calculated amount of absorbed hydrogen during the absorption measurements for $LiBH_4$-MgH_2-Al (4:1:1, **S1**) and $LiBH_4$-MgH_2-Al (4:1:5, **S2**).*

Sample	**Absorption #**	**1**	**2**	**3**
S1, $LiBH_4$-MgH_2-Al (4:1:1) [wt% H_2]		7.8	6.4	5.6
S2, $LiBH_4$-MgH_2-Al (4:1:5) [wt% H_2]		5.5	3.8	3.5

* The absorbed wt% hydrogen is calculated from the difference in pressure at *RT* before and after heating the sample.

Table 5. Molar composition determined from ^{11}B MAS NMR for the samples $LiBH_4$-MgH_2-Al (4:1:1, **S1**) and $LiBH_4$-MgH_2-Al (4:1:5, **S2**) after three hydrogen release and uptake cycles applying different hydrogen backpressure during desorption.

Sample	$Li_2B_{12}H_{12}$ (mol%)	$LiBH_4$ (mol%)
S1, $p(H_2)$ = 0.15 bar	19.1	80.9
S1, $p(H_2)$ = 5.0 bar	8.7	91.3
S2, $p(H_2)$ = 0.15 bar	8.0	92.0
S2, $p(H_2)$ = 5.0 bar	2.4	97.6

***Phys. Chem. Chem. Phys.*, 2014, Revised**

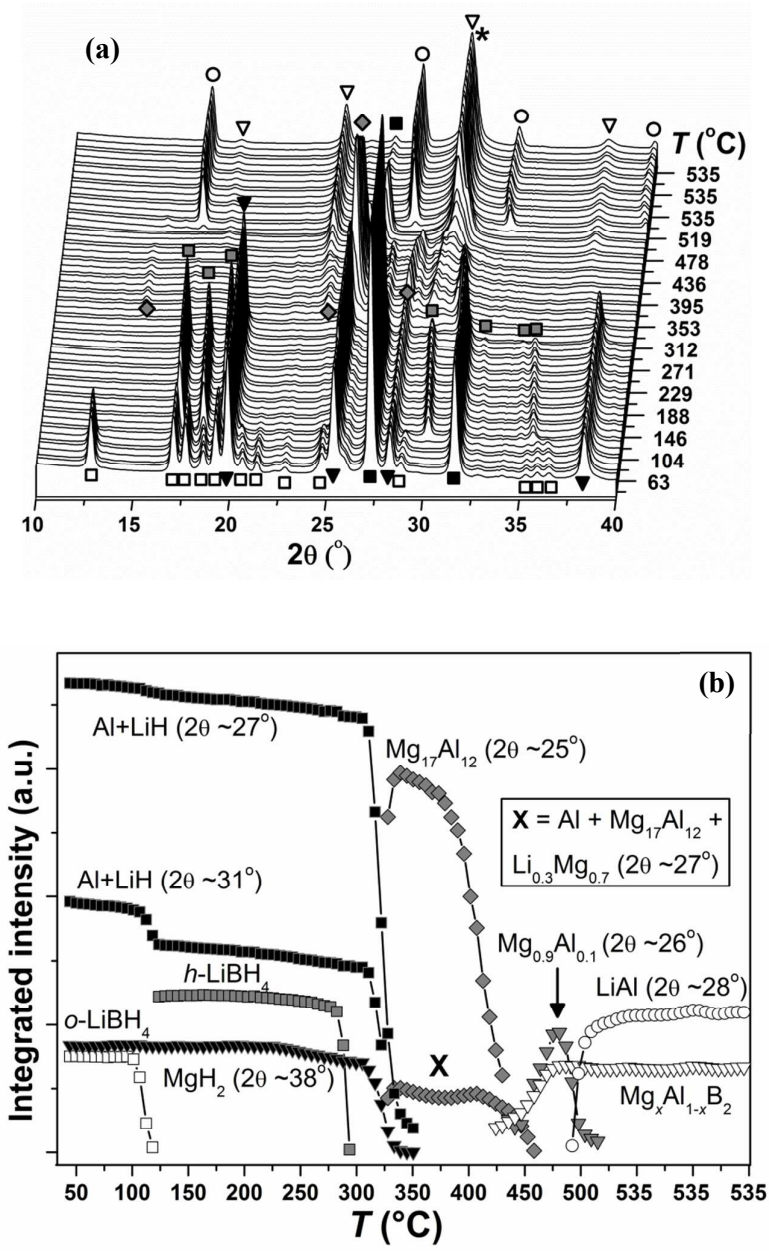

Figure 1 (a) *In situ* SR-PXD desorption measurements for $LiBH_4$-MgH_2-Al (4:1:1, **S1**) in the temperature range from *RT* to 535 °C, at $p(H_2) = 10^{-2}$ bar ($\Delta T/\Delta t$ = 10 °C/min, λ = 1.103671 Å). The sample was kept at a constant temperature of 535 °C for 15 min. **(b)** Integrated diffracted intensities of selected data from (a). Symbols: □ *o*-$LiBH_4$, ■ *h*-$LiBH_4$, ■ Al, ▼ MgH_2, ◆ $Mg_{17}Al_{12}$, ▼ $Mg_{0.9}Al_{0.1}$, ▽ $Mg_xAl_{1-x}B_2$, * MgO and ○ LiAl.

***Phys. Chem. Chem. Phys.*, 2014, Revised**

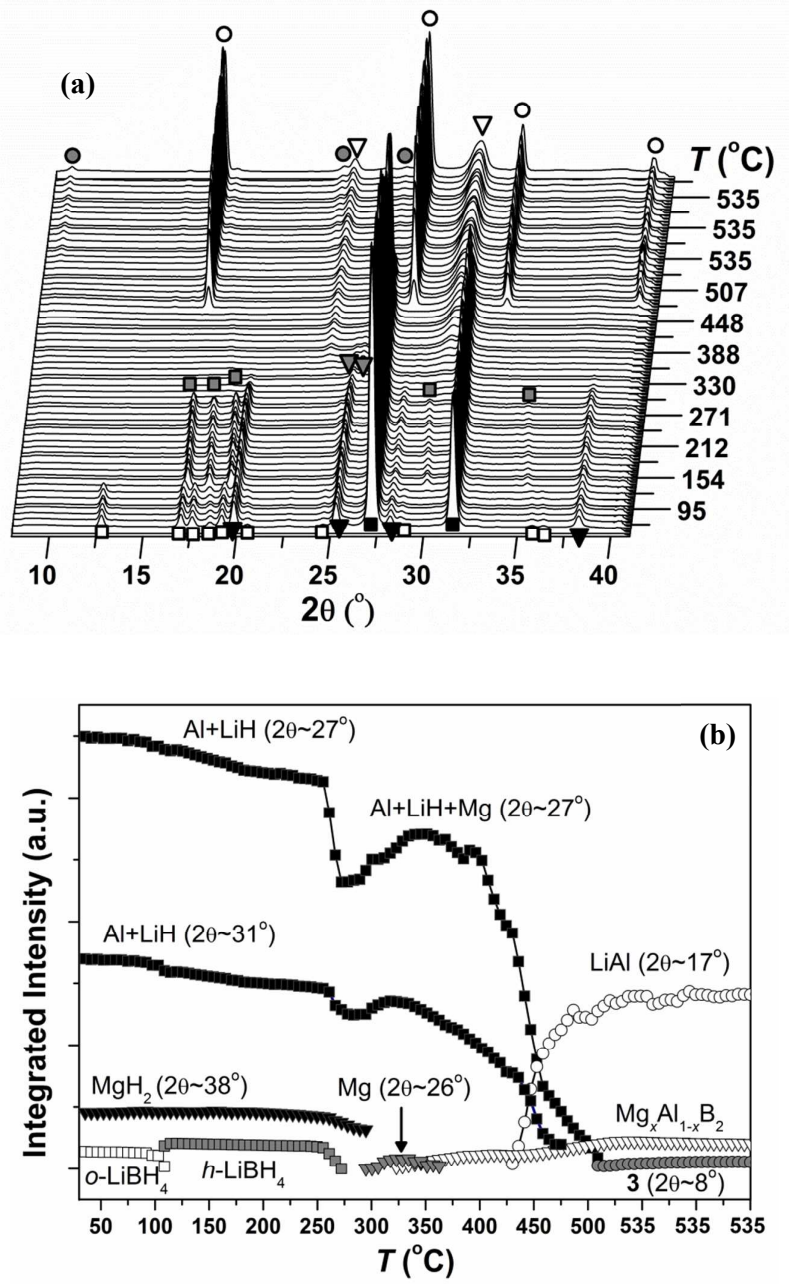

Figure 2 (a) *In situ* SR-PXD desorption measurements for $LiBH_4$-MgH_2-Al (4:1:5, **S2**) in the temperature range from *RT* to 535 °C, at $p(H_2) = 10^{-2}$ bar ($\Delta T/\Delta t$ = 10 °C/min, λ = 1.102050 Å). The sample was kept at a constant temperature of 535 °C for 15 min. **(b)** Integrated diffracted intensities of selected data from (a). Symbols: □ *o*-$LiBH_4$, ■ *h*-$LiBH_4$, ■ Al, ▼ MgH_2, ▼ Mg, ▽ $Mg_xAl_{1-x}B_2$, ○ LiAl and ● **3**.

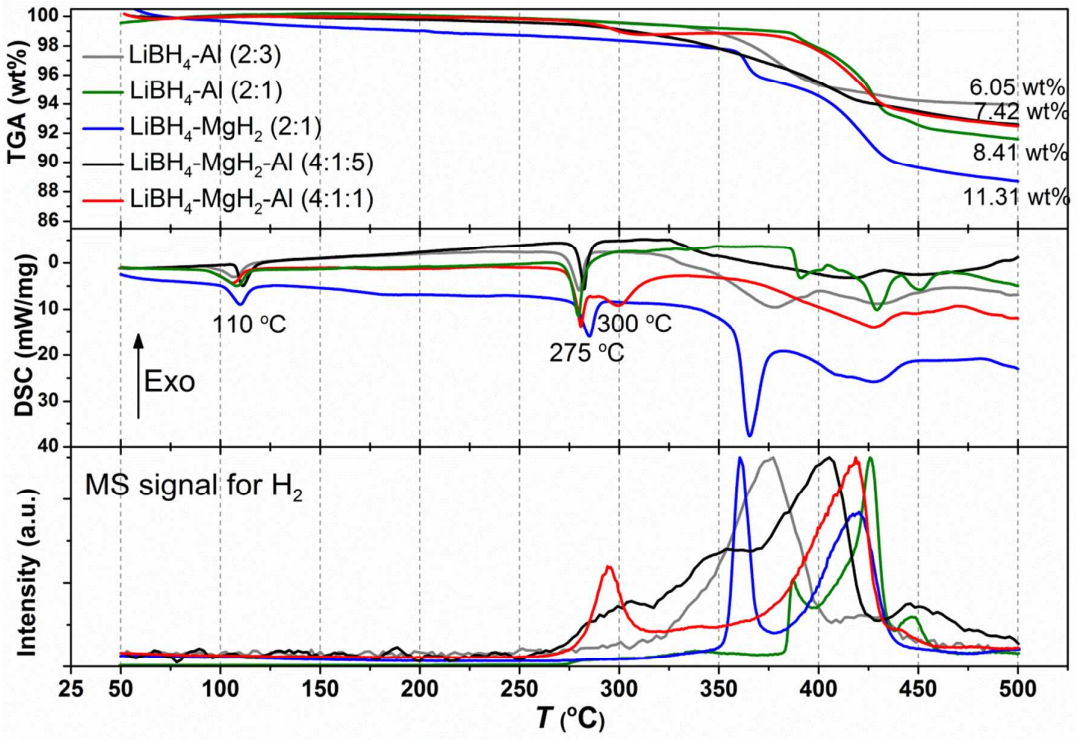

Figure 3. TGA-DSC-MS profiles for samples **S1-S5** in the temperature range 50 - 500 °C ($\Delta T/\Delta t$ = 5 °C/min, Ar flow).

***Phys. Chem. Chem. Phys.*, 2014, Revised**

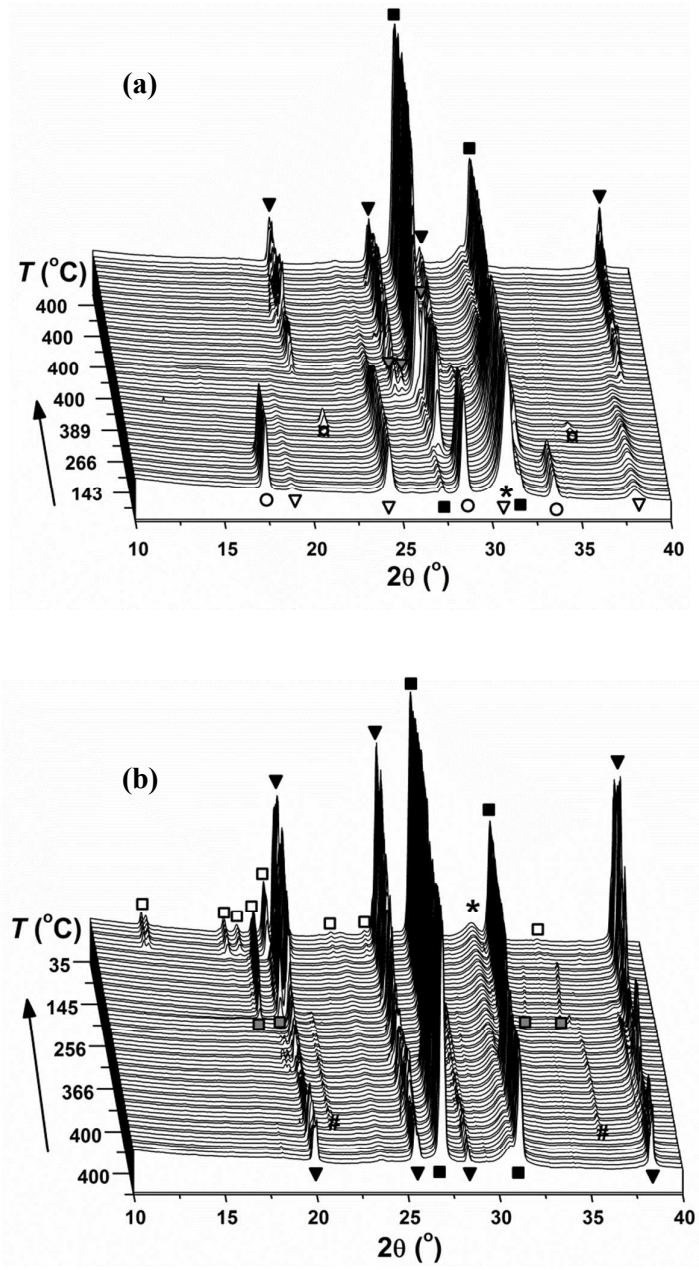

Figure 4. *In situ* SR-PXD hydrogen absorption measurements for $LiBH_4$-MgH_2-Al (4:1:1, **S1**, decomposed) at $p(H_2)$ = 100 bar in the temperature range from **(a)** *RT* to 400 °C ($\Delta T/\Delta t$ = 15 °C/min). **(b)** The sample was kept at a constant temperature of 400 °C for 60 min and then cooled to *RT* ($\Delta T/\Delta t$ = -10 °C/min) (λ = 1.103671 Å). Symbols: □ *o*-$LiBH_4$, ■ *h*-$LiBH_4$, ■ Al, ▼ MgH_2, ▼ Mg, ▽ $Mg_xAl_{1-x}B_2$, * MgO, ○ LiAl, ¤ **1** and # **2**.

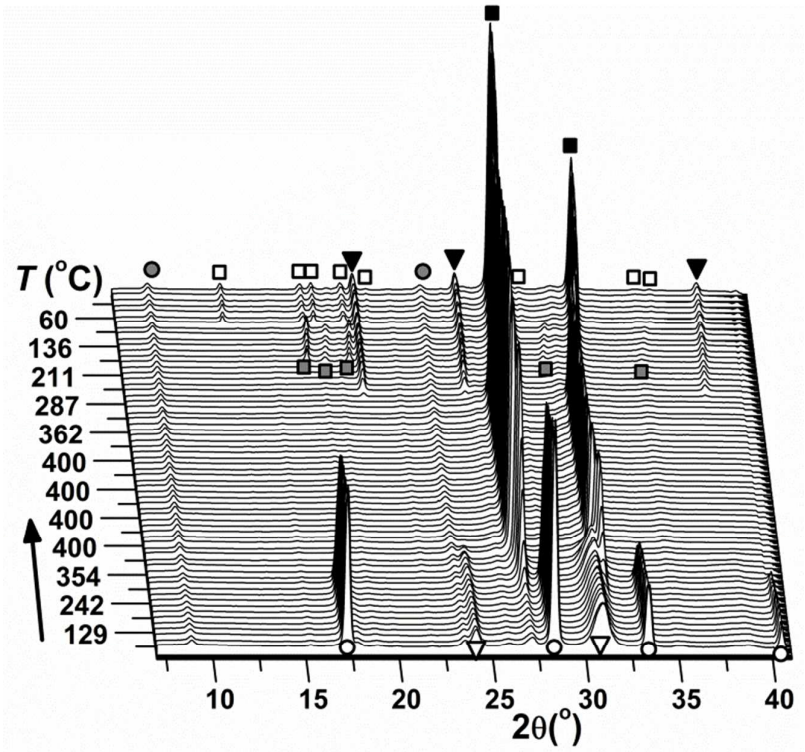

Figure 5. *In situ* SR-PXD hydrogen absorption measurements for $LiBH_4$-MgH_2-Al (4:1:5, **S2**, decomposed) in the temperature range from *RT* to 400 °C, at $p(H_2)$ = 100 bar ($\Delta T/\Delta t$ = 15 °C/min, λ = 1.102050 Å). The sample was kept at a constant temperature of 400 °C for 60 min before cooling to *RT* ($\Delta T/\Delta t$ = -10 °C/min). Symbols: □ *o*-$LiBH_4$, ■ *h*-$LiBH_4$, ■ Al, ▼ MgH_2, ▽ $Mg_xAl_{1-x}B_2$, ○ LiAl and ● **3**.

***Phys. Chem. Chem. Phys.*, 2014, Revised**

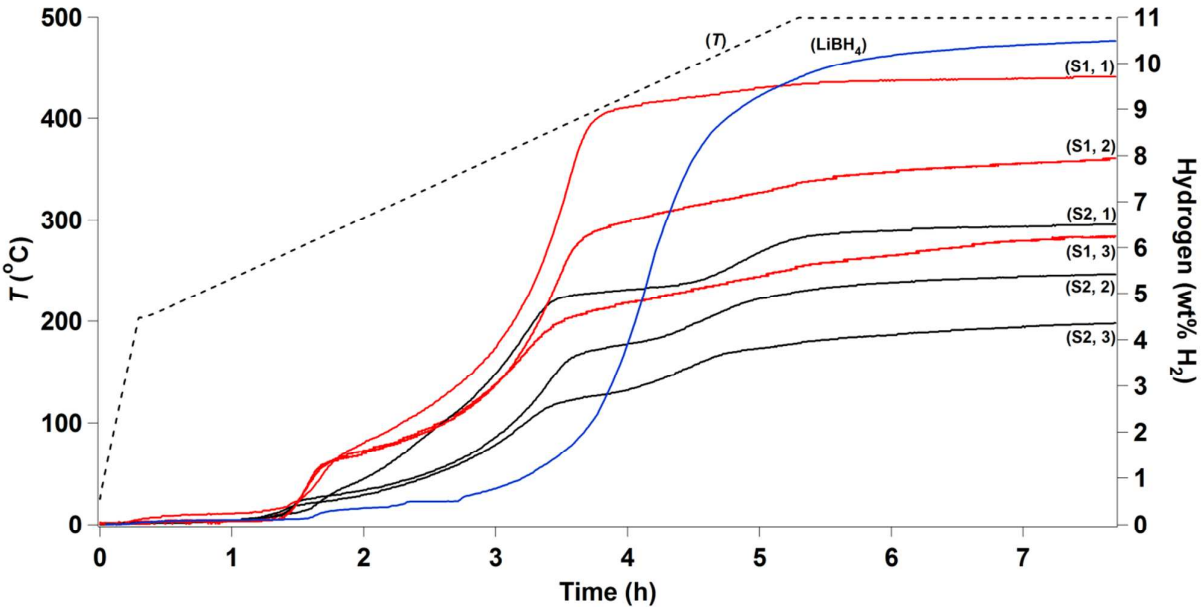

Figure 6. Desorption measurements for $LiBH_4$-MgH_2-Al (4:1:1, **S1**), $LiBH_4$-MgH_2-Al (4:1:5, **S2**) and $LiBH_4$. The dashed line is the temperature profile and the desorptions are numbered **S1** or **S2**, 1 - 3. Pristine $LiBH_4$ is measured for comparison. The samples were heated to 200 °C ($\Delta T/\Delta t$ = 10 °C/min) and subsequently to 500 °C ($\Delta T/\Delta t$ = 1 °C/min), where the temperature was maintained for 150 min, in $p(H_2)$ = 0.15 bar.

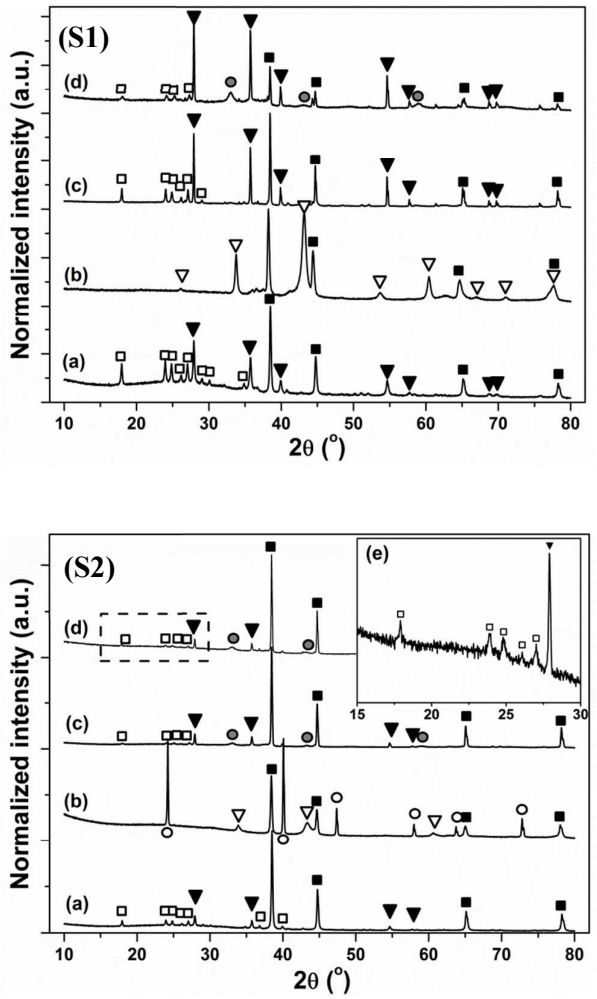

Figure 7. Diffractograms of $LiBH_4$-MgH_2-Al (4:1:1, **S1**) and $LiBH_4$-MgH_2-Al (4:1:5, **S2**) after (a) ball milling, (b) first desorption in PCT and (c) first absorption in PCT (d) third absorption in PCT (e) shows a magnified view of the dashed box in (**S2**(d)) (λ = 1.54056 Å). Symbols: □ *o*-$LiBH_4$, ■ Al, ▼ MgH_2, ▽ $Mg_xAl_{1-x}B_2$ and ● Unknown **3**.

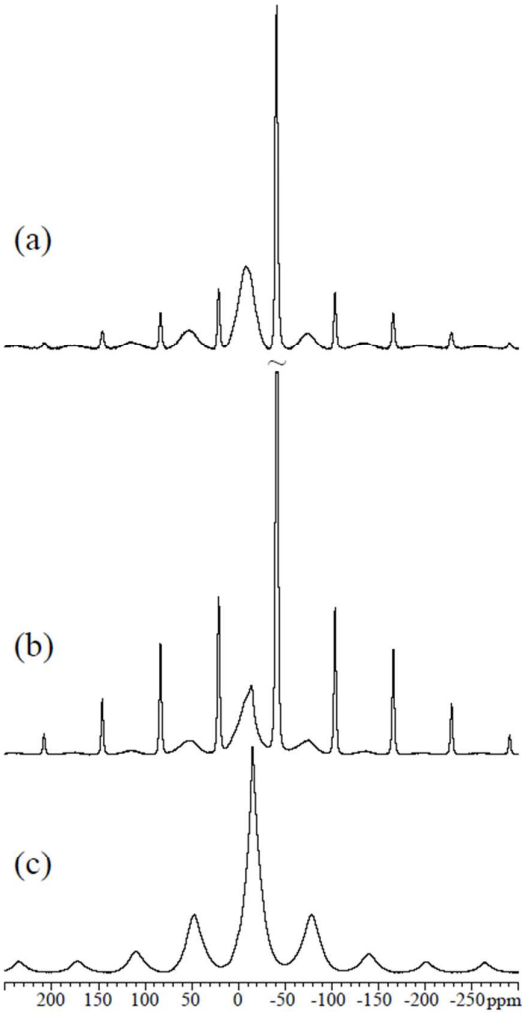

Figure 8. ^{11}B MAS NMR spectra (14.1 T, ν_R = 12.0 kHz) for the sample **S1** after three Sieverts cycles using hydrogen partial pressures of (a) $p(H_2)$ = 0.15 bar and (b) $p(H_2)$ = 5 bar during hydrogen desorption (*RT* to 500 °C), while absorption is performed using similar conditions in (a) and (b), and of (c) a pure sample of for $Li_2B_{12}H_{12}$. The central transition centerbands for $LiBH_4$ and $Li_2B_{12}H_{12}$ are observed at −41.3 ppm and −9 ppm, respectively.

***Phys. Chem. Chem. Phys.*, 2014, Revised**

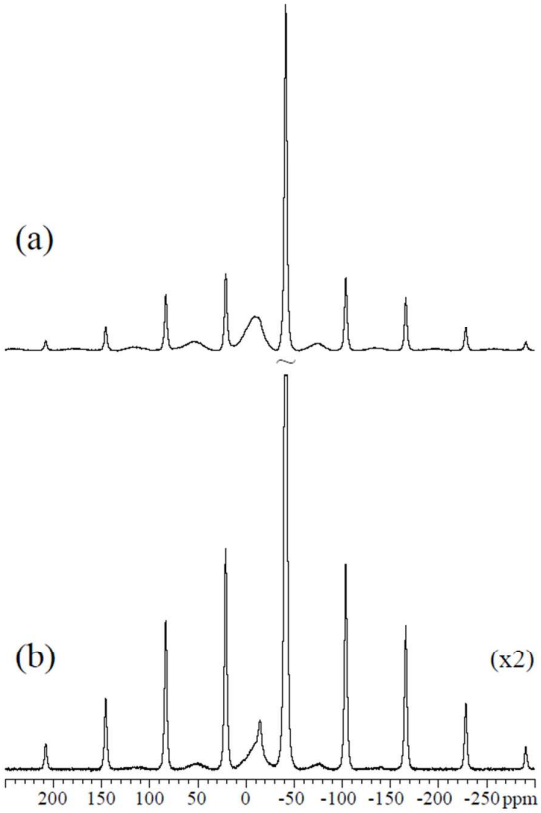

Figure 9. ^{11}B MAS NMR spectra (14.1 T, ν_R = 12.0 kHz) for the **S2** sample after three Sieverts cycles using hydrogen partial pressures of (a) $p(H_2)$ = 0.15 bar and (b) $p(H_2)$ = 5 bar during hydrogen desorption (*RT* to 500 °C), while absorption is performed using similar conditions for the samples in (a) and (b).

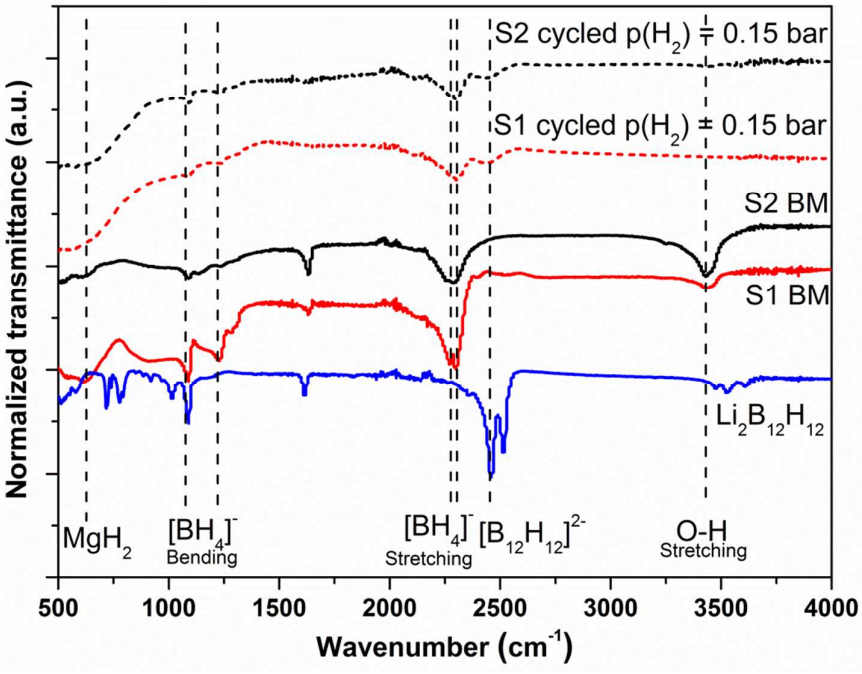

Figure 10. FT-IR spectra of ball-milled and cycled **S1** and **S2** samples in the frequency range of 500 to 4000 cm^{-1}. A measurement of crystalline, anhydrous $Li_2B_{12}H_{12}$ is presented for comparison of the $B_{12}H_{12}^{2-}$ vibrations.

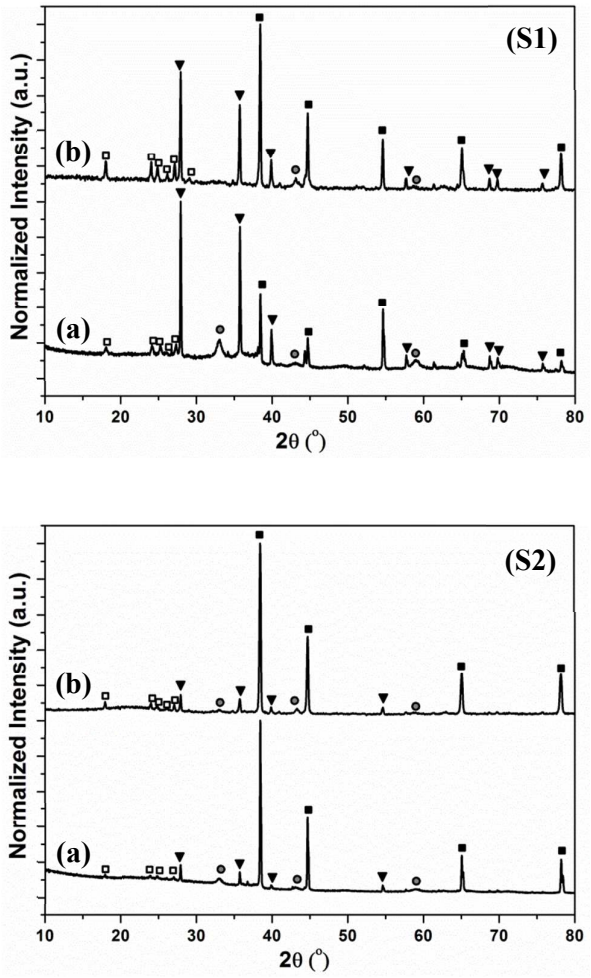

Figure 11. (S1) Diffractograms of $LiBH_4$-MgH_2-Al (4:1:1, **S1**) and **(S2)** $LiBH_4$-MgH_2-Al (4:1:5, **S2**) obtained after three hydrogen release and uptake cycles where hydrogen release was performed with (a) $p(H_2)$ = 0.15 bar and (b) $p(H_2)$ = 5 bar (λ = 1.54056 Å). Symbols: □ *o*-$LiBH_4$, ■ Al, ▼ MgH_2 and ● **3**.